Chemical Engineering and Processing 122 (2017) 331–338

Contents lists available at ScienceDirect

Chemical Engineering and Processing: Process Intensification

journal homepage: www.elsevier.com/locate/cep

Localized microwave-heating intensification—A 1-D model and potential applications

Eli Jerby

Faculty of Engineering, Tel Aviv University, Ramat Aviv 6997801, Israel

ARTICLE INFO

Article history:
Received 15 July 2016
Accepted 21 February 2017
Available online 24 February 2017

Keywords:
Microwave heating
Intensification
Hotspot
Drilling
Fireball
Sintering
Thermite
Ignition
3D printing

ABSTRACT

This paper reviews the localized microwave-heating (LMH) phenomenon and its various applications in a paradigmatic approach. A simplified 1-D microwave-heating model is derived for a temperature-dependent dielectric medium in a cavity. This semi-analytical model shows the evolution of high-order spatial modes, and the concentration therein of the dissipated power. The LMH effect is associated with the localized hotspot formation due to the thermal-runaway instability. LMH intensification in solids and powders enables various applications using the microwave-drill technique, as reviewed in this paper. These include for instance local heating, up to $>10^3$ K, also by LDMOS transistors; ignition of thermite powders in air atmosphere and underwater; generation of plasma columns and spheres from molten hotspots in solids (*e.g.* silicon, titanium), and production of nano-powders by dusty plasma. The potential for 3D-printing and additive manufacturing (AM), recently demonstrated by local solidification of metal powders in a stepwise manner by LMH, is discussed.

1. Introduction

Microwave heating is typically implemented in uniformly-distributed schemes, *e.g.* in ovens, conveyer applicators, and furnaces. The heat-affected zone (HAZ) in these systems is usually comparable in size to the microwave wavelength (*e.g.* 12.2 cm at 2.45-GHz frequency) or larger [1,2]. Non-uniform heating patterns may accidentally evolve in such volumetric processes [3], and rapidly create hotspots. The high temperatures evolved in these accidental hotspots might be harmful in applications which require moderate uniform heating, such as processing of food or drying applications [4,5].

Thermal-runaway instabilities and localized microwave-heating (LMH) effects [6–9] may occur in materials characterized by temperature-dependent properties (which dictate faster energy absorption than heat diffusion rate). Localized heating effects tend to occur in materials of which the dielectric loss increases with temperature (and/or the thermal conductivity decreases). The initial non-uniform heating due to the radiation pattern modifies the spatial distribution of the material properties, which further increases the microwave absorption there, in an unstable positive-feedback manner [10]. The LMH instability is terminated at the material phase transition within the hotspot; to a liquid, gas or even plasma state. The HAZ size is determined by the material properties, the microwave wavelength and power, and the applicator geometry. This HAZ size could be much smaller than the microwave wavelength, λ, hence the local heating effect there is accordingly intensified. The microwave drill [11] intentionally utilizes the LMH effect by purposely exciting thermal-runaway instability [12]. It generates a small hotspot (with a diameter $\sim 10^2$ shorter than λ), which enables local temperature increase to >1000 °C in heating rates of >100 °C/s. LMH effects have been demonstrated by microwave drills in concrete, ceramics, basalts, glass, polymers, silicon, and other materials [13–19]. LMH may also be useful for microwave-assisted mining [20] and concrete-recycling [21] applications.

Various LMH effects have been investigated for medical applications, such as tissue heating [22], bone drilling [23], interstitial treatments [24,25], ablation for cancer therapy [26–28] and DNA-amplification studies [29]. LMH may also play a significant role in chemical and electro-chemical reactions [30,31]. In particular, open-end coaxial microwave applicators are used for direct heating of liquid [32] and for activation of chemical reactions [33]. An LMH doping effect [34] was demonstrated with silver and aluminum dopants locally diffused by LMH into silicon to form a diode PN-junction. It was also shown that LMH may generate dusty plasma, in forms of fire-columns and fireballs (plasmoids), directly from solid substrates [35], and produce nano-particles [36–39].

E-mail address: jerby@eng.tau.ac.il (E. Jerby).

http://dx.doi.org/10.1016/j.cep.2017.02.008
0255-2701/

The typical hotspot size in solids referred to in this paper is in the order of ~1 mm or larger (note that other LMH effects may also occur in powder mixtures in the micrometric scale, *e.g.* [40]). The LMH effect can be spatially directed and intensified by a proper concentrating applicator, such as an open-end electrode (as employed in microwave drills [11–19] and in chemical reactors [30,32,33]), or by localized susceptors (as in [41]). Otherwise, LMH may be spontaneously initiated even in seemingly uniform cavities, as analyzed in the next section.

Due to the significant energy concentration, the LMH effect can be implemented by a relatively low power (in the order of ~0.1 kW) generated by a transistor-based microwave heater (as demonstrated by LDMOS microwave drills [42]). This solid-state technology opens new possibilities for compact LMH devices. It could be useful for ignition (*e.g.* of thermite reactions [43]), local sintering of metal powders, additive manufacturing and 3D-printing [44], mold heating and casting [45], and material identification [46]. In such applications, LMH may also provide a low-cost substitute for laser-based techniques. This paper introduces a 1-D model of the fundamental LMH intensification effect in a uniform cavity, and reviews various theoretical, experimental, and practical aspects of the LMH paradigm [47–49].

2. A 1-D modal analysis of LMH intensification

LMH models (*e.g.* [10,12,43]) are governed in general by the electromagnetic (EM) wave equation and the heat equation,

$$\nabla \times \left(\mu_r^{-1}\nabla \times \tilde{\mathbf{E}}\right) - \varepsilon_r k_0^2 \tilde{\mathbf{E}} = -jk_0 Z_0 \tilde{\mathbf{J}}, \tag{1}$$

$$\rho c_p \partial T/\partial t - \nabla \cdot (k_{th}\nabla T) = Q_d, \tag{2}$$

coupled together by the temperature dependent parameters and by the EM-heat dissipated power density,

$$Q_d = \frac{1}{2}\left[(\sigma + \omega\varepsilon_0\varepsilon_r'')|\tilde{\mathbf{E}}|^2 + \omega\mu_0\mu_r''|\tilde{\mathbf{H}}|^2\right], \tag{3}$$

where $\tilde{\mathbf{E}}$ and $\tilde{\mathbf{H}}$ are the electric- and magnetic-field vector components of the EM wave ($\tilde{\mathbf{H}} = j\nabla \times \tilde{\mathbf{E}}/\omega\mu_0\mu_r$), and T is the temperature evolved in the process. The EM fields are presented as phasors in the frequency domain, where ω and k_0 are the angular frequency and free-space wave-number, respectively ($k_0 = \omega\sqrt{\varepsilon_0\mu_0}$). The EM wave excitation is represented by the displacement-current vector, $\tilde{\mathbf{J}}$, where $Z_0 = \sqrt{\mu_0/\varepsilon_0}$ is the free-space characteristic impedance. The heated medium is characterized by its temperature-dependent parameters, μ_r, ε_r, σ, ρ, c_p, and k_{th}, where $\varepsilon_r = \varepsilon_r' - j\varepsilon_r''$ and $\mu_r = \mu_r' - j\mu_r''$ are its relative complex dielectric-permittivity and magnetic-permeability, respectively, and σ is its electric conductivity. In the heat equation (2), ρ, c_p and k_{th} are the medium's actual density, specific heat capacity, and thermal conductivity, respectively, which may be non-uniformly changed due to the LMH effect. It is noted though that the temperature profile T is slowly varying with respect to the EM wave. The distinction between the typical time scales of the EM wave propagation (~1 ns) and the much slower thermal evolution (>1 ms) allows the *two-time scale* approximation [12], hence the solution of the heat equation (2) in the time domain.

2.1. A 1-D microwave-applicator model

The LMH effect is demonstrated here in a simplified case of a 1-D resonator used as a microwave-heating applicator (assuming ∂_x, $\partial_y = 0$ and $\mu = \mu_0$). The resonator illustrated in Fig. 1a is uniformly filled with a lossy dielectric medium. Fig. 1b shows *(i)* the temperature dependence of the complex dielectric permittivity (typically increased with temperature as in many materials). The initial electric-field profile in the cavity *(ii)* leads to a non-uniform heating pattern *(iii)* which makes the hotter region more susceptible to further microwave heating due to its permittivity increase *(iv)*. A thermal-runaway instability is consequently evolved, which leads to a hotspot formation, as mentioned above [6–12].

The resonator is excited by an effective displacement current, $\tilde{\mathbf{J}} = \hat{\mathbf{x}}\tilde{J}_x(z)$, hence the electric field evolved, $\tilde{\mathbf{E}} = \hat{\mathbf{x}}\tilde{E}_x(z)$, is found by

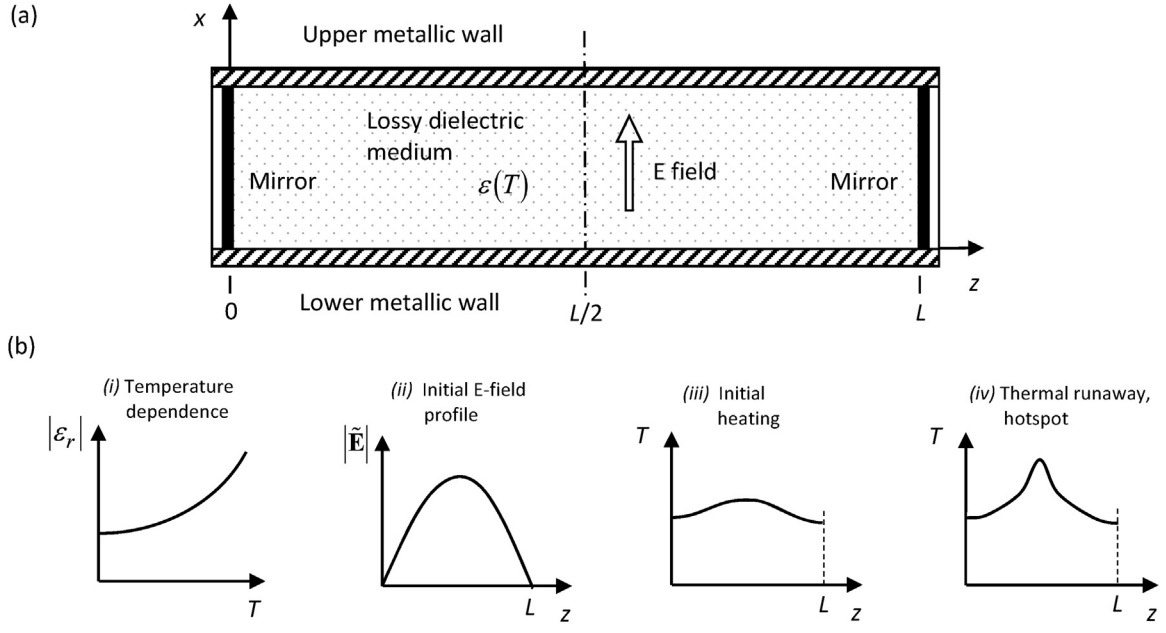

Fig. 1. (a) A 1-D microwave resonator filled with a lossy dielectric medium, as assumed for this analysis. (b) An illustration of a typical LMH process enabled by the temperature-dependence of the dielectric permittivity *(i)* and intiated by the spatially non-uniform electric-field profile *(ii)*. The initial heating pattern *(iii)* modifies the dielectric permitivity profile according to *(i)*, which further enhance the localized abosrption of the microwave power. The thermal-runaway instability leads to the evolution of a confined hotspot *(iv)*.

the 1-D wave equation derived from (1),

$$\partial_z^2\tilde{E}_x + k_0^2 g\tilde{E}_x = jk_0 Z_0\tilde{J}_x, \tag{4}$$

where the normalized profile $g(z,t)$ of the slowly-varying complex dielectric medium is defined as

$$g(z,t) = \varepsilon(T(z,t))/\varepsilon_0. \tag{5}$$

Assuming that the excitation current $\tilde{J}_x$ and consequently the excited field $\tilde{E}_x(z)$ are symmetrical around $L/2$ (and both vanish at $z=0$ and L), they are expanded by Fourier series as follows:

$$\tilde{E}_x(z) = \sum_{n=1,3,5\ldots}\tilde{\bar{E}}_n\sin\left(n\pi\frac{z}{L}\right), \tag{6a}$$

$$\tilde{J}_x(z) = \sum_{n=1,3,5\ldots}\tilde{\bar{J}}_n\sin\left(n\pi\frac{z}{L}\right). \tag{6b}$$

The dielectric profile function is also symmetrical around $L/2$ but is non-zero at $z=0$ and $z=L$, hence

$$g(z) = \frac{1}{2}\bar{g}_0 + \sum_{n=2,4,6\ldots}\bar{g}_n\cos\left(n\pi\frac{z}{L}\right). \tag{7}$$

This expansion employs the *method of images*, as in Refs. [50,51]. The discrete spatial-spectrum coefficients $\tilde{\bar{E}}_n$ are given therefore by the integral,

$$\tilde{\bar{E}}_n = \frac{2}{L}\int_{z=0}^{L}\tilde{E}_x(z)\sin\left(n\pi\frac{z}{L}\right)dz. \tag{8}$$

It represents the axial modes, evolved in the resonator due to the interaction with the varying dielectric medium, as illustrated in Fig. 2.

The 1-D wave equation (4) is rewritten in terms of the Fourier series expansion (6, 7) in the form

$$\sum_{n=1,3,5\ldots}\left(\frac{n\pi}{L}\right)^2\tilde{\bar{E}}_n\sin\left(n\pi\frac{z}{L}\right) - \frac{k_0^2}{2}\sum_{n=1,3,5\ldots}\tilde{\bar{E}}_n\left\{\bar{g}_0\sin\left(n\pi\frac{z}{L}\right) + \sum_{m=2,4,6\ldots}\bar{g}_m\left[\sin\left(\frac{n-m}{L}\pi z\right) + \sin\left(\frac{n+m}{L}\pi z\right)\right]\right\} = -jk_0Z_0\sum_{n=1,3,5\ldots}\tilde{\bar{J}}_n\sin\left(n\pi\frac{z}{L}\right), \tag{9}$$

with the convolution term $\sum_n\ldots\sum_m\ldots$ resulted from the product $g(z)\tilde{E}_x(z)$ in the spatial domain, in the wave equation (4).

A further elaboration, using the orthogonality feature of the sine and cosine functions (multiplying both sides of Eq. (9) by $\sin(l\pi z/L)$, and integrating over $\int_{z=0}^{L}\ldots$) and setting $g_n=0$ for $n<0$, results in a simplified wave equation for the l-th axial mode ($l=1,3,5\ldots$) in the form

$$\left(\frac{l\pi}{L}\right)^2\tilde{\bar{E}}_l - k_0^2\left(\sum_{n=1,3,5\ldots}^{l}\bar{g}_{l-n}\tilde{\bar{E}}_n + \sum_{n=l+2,l+4\ldots}^{\infty}\bar{g}_{n-l}\tilde{\bar{E}}_n\right) = -jk_0Z_0\tilde{\bar{J}}_l. \tag{10}$$

Equation (10) is further compacted to the matrix wave-equation,

$$\left[\left(\frac{\pi}{L}\right)^2\underline{\underline{\mathbf{L}}} - k_0^2\underline{\underline{\mathbf{G}}}\right]\underline{\mathbf{E}} = -jk_0Z_0\underline{\mathbf{J}}, \tag{11}$$

where the *convolution matrix*, $\underline{\underline{\mathbf{G}}}$, and the diagonal matrix of the modal indices, $\underline{\underline{\mathbf{L}}}$, are defined here as

$$\underline{\underline{\mathbf{G}}} = \begin{bmatrix}\bar{g}_0 & \bar{g}_2 & \bar{g}_4 & \cdots\\ \bar{g}_2 & \bar{g}_0 & \bar{g}_2 & \cdots\\ \bar{g}_4 & \bar{g}_2 & \bar{g}_0 & \cdots\\ \vdots & \vdots & \vdots & \ddots\end{bmatrix}, \qquad \underline{\underline{\mathbf{L}}} = \begin{bmatrix}1 & 0 & 0 & \cdots\\ 0 & 3^2 & 0 & \cdots\\ 0 & 0 & 5^2 & \cdots\\ \vdots & \vdots & \vdots & \ddots\end{bmatrix} \tag{12a, b}$$

respectively. The vectors $\underline{\mathbf{J}}$ and $\underline{\mathbf{E}}$, which consist of the spatial-spectrum components of the excitation current and the electric field, respectively, are defined as

$$\underline{\mathbf{E}} = \begin{bmatrix}\tilde{\bar{E}}_1\\ \tilde{\bar{E}}_3\\ \tilde{\bar{E}}_5\\ \vdots\end{bmatrix}, \qquad \underline{\mathbf{J}} = \begin{bmatrix}\tilde{\bar{J}}_1\\ \tilde{\bar{J}}_3\\ \tilde{\bar{J}}_5\\ \vdots\end{bmatrix} \tag{13a, b}$$

The evolution of the electric-field axial modes, caused by the non-uniform heating and by the consequent variation in the $g(z)$ profile, is found by the matrix relation

$$\underline{\mathbf{E}} = \frac{1}{j\omega_0\varepsilon_0}\left[\left(\frac{\lambda_0}{2L}\right)^2\underline{\underline{\mathbf{L}}} - \underline{\underline{\mathbf{G}}}\right]^{-1}\underline{\mathbf{J}}. \tag{14}$$

The heat equation (2) describes the temporal and spatial evolution of the local temperature $T(z,t)$, and therefore enables to find the actual dielectric profile, $g(T(z,t))$. In this simplified 1-D case, Eq. (2) is reduced to the form

$$\rho c_p\partial_t T - k_{th}\partial_z^2 T = Q_d, \tag{15}$$

where ρ, c_p and k_{th} are assumed here as independent of temperature. The power density due to the dielectric heating is given by

$$Q_d = \frac{1}{2}\omega\varepsilon_0\varepsilon_r''|\tilde{E}_x|^2. \tag{16}$$

The simplified heat-equation also neglects the blackbody radiation. The boundaries at $z=0$ and L are assumed to maintain the initial (ambient) temperature, T_0. The slowly-varying temperature profile $T(z,t)$ and the dissipated power density Q_d are expanded as well by the following Fourier series,

$$T(z,t) = T_0 + \sum_{n=1,3,5\ldots}\bar{T}_n(t)\sin\left(n\pi\frac{z}{L}\right), \tag{17a}$$

$$Q_d(z,t) = \sum_{n=1,3,5\ldots}\bar{Q}_n(t)\sin\left(n\pi\frac{z}{L}\right), \tag{17b}$$

hence the heat equation (15) attains the form

$$\rho c_p\frac{d}{dt}\bar{T}_n(t) + k_{th}\left(\frac{n\pi}{L}\right)^2\bar{T}_n(t) = \bar{Q}_n(t). \tag{18}$$

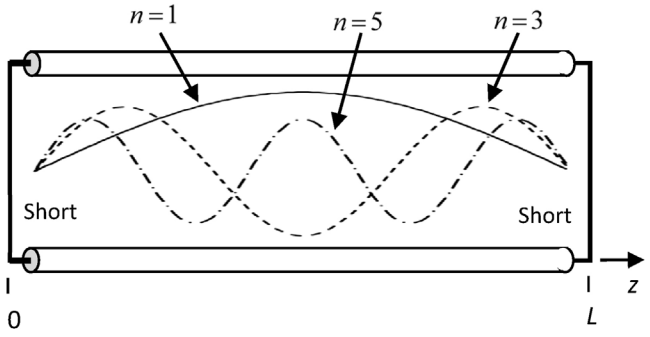

Fig. 2. Odd-order axial modes ($n=1, 3, 5\ldots$) evolved in an equivalent resonator (a transmission-line shortened at both ends) due to the LMH interaction.

The slowly-varying time domain is discretized by finite differences, thus $d\overline{T}_n(t)/dt \cong \Delta\overline{T}_n/\Delta t$, and Eq. (18) yields

$$\overline{T}_n(t+\Delta t) \cong \overline{T}_n(t) + \left[\overline{Q}_n(t) - (n\pi/L)^2 k_{th}\overline{T}_n(t)\right]\Delta t/\rho c_p. \quad (19)$$

The temperature $T(z,t)$ is reconstructed at each computing step $t+\Delta t$ by Eq. (17a), and the dielectric profile $g(z,t)$ is updated accordingly for the next round of EM calculation (14).

2.2. A numerical example of LMH intensification in a 1-D resonator

As an example for the LMH intensification effect, a 1-D resonator is assumed to be filled with a dielectric medium of $\varepsilon_r = (4 - j0.02)\cdot\left[1 + (T/300 - 1)^2\right]$ for $T \geq T_0 = 300$ K, $\rho c_p = 1$ J/cm^{3}K, and $L = 6$ cm. The resonator is excited by a 2.45-GHz microwave generator (~1 kW), and the non-resonating fundamental axial mode $n = 1$ is imposed by the equivalent current-density profile, $\tilde{J}_x(z)$.

The coupled solution of Eqs. (14) and (19) shows that higher-order modes are dynamically evolved during the non-uniform microwave heating, as shown in Fig. 3. The temperature-dependent dielectric permittivity, consequently modified along the resonator, is coupled to the higher-order modes. These enable the sharper sub-wavelength intensification of the EM dissipated power $Q_d(z,t)$, initially distributed as the original fundamental mode (with a $\sin^2(\pi z/L)$ profile). As the LMH instability proceeds, Q_d becomes significantly intensified and confined at the hotspot region, as shown in Fig. 4. The localized temperature profile is sharpened accordingly to intensify the hotspot, as shown in Fig. 5.

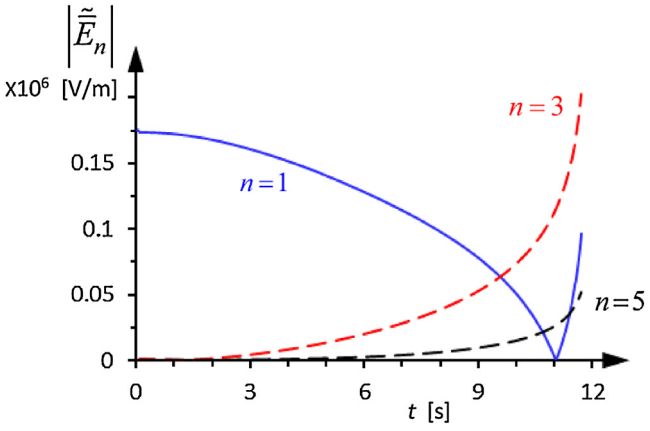

Fig. 3. The axial-mode dynamics evolved in the resonator during the LMH process.

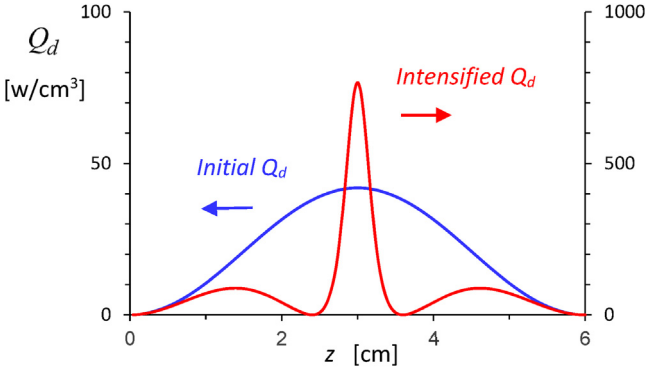

Fig. 4. The initial and final profiles of the dispated power density, from the fundamental-mode excitation to the LMH-intensified microwave power dissipation at the hotspot.

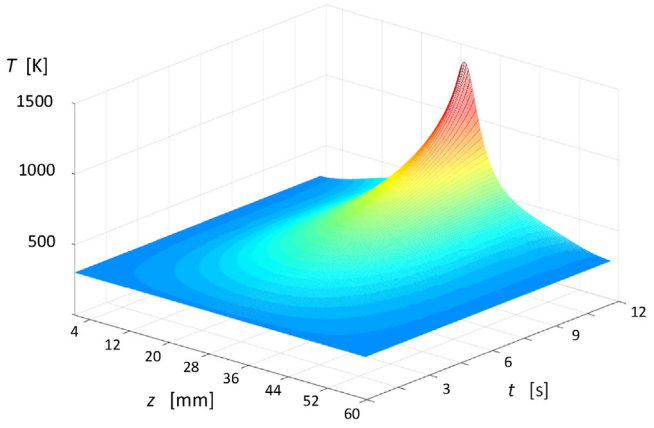

Fig. 5. The localized microwave-heating profile evolved along the resonator, and the hotspot intensification by the LMH thermal-runaway instability.

3. LMH intensification in applicable processes

The LMH intensification effect enables a wide range of applications in a variety of fields, as reviewed in the Introduction section above. Several applicative aspects are further discussed in more detail in this section.

3.1. Heat intensification in a microwave cavity

The LMH intensification due to the temperature-dependent material properties (as shown *e.g.* in Fig. 1b) can be demonstrated for instance by irradiating a basalt brick in a microwave cavity [52]. The heat intensification effect is clearly seen as the basalt brick is melted inside while its outer surface remains solid, as shown in Fig. 6a, b. The molten core ejects lava outside the brick, which leaves a void inside (whereas the outer surface of the brick remains solid). A 3D multi-physics model, using equations (1–3), agrees well with the temperature profiles measured on the basalt brick faces [52]. Similar demonstrations are also conducted with natural-shape basalt stones, to mimic various volcanic phenomena in a laboratory scale [52]. This LMH effect can be further used in order to intensify extraction processes.

3.2. Open-end applicator for LMH intensification

The LMH intensification can be even more effectively localized by a waveguide (*e.g.* an open-end coaxial applicator) as compared to the uniform resonator presented above. This additional means for further intensification has been demonstrated in various materials, *e.g.* by microwave-drill experiments [11,13–19]. A silent microwave-drill for concrete was recently developed [53] with the capability to drill 12-mm diameter, >25-cm deep holes. Delicate microwave drilling operations were also demonstrated (in a ~1-mm diameter range), for instance by relatively low-power (~0.1 kW) LMH applied to soda-lime glass plates (of 1–4 mm thickness) [42]. The simulation of the LMH evolution in these cases by Eqs. ((1)–(3)), using Comsol Multiphysics™, agrees well with the experimental measurements [42]. A simulated hotspot profile is shown for instance in Fig. 7, with an image of a hole made in glass by a miniature microwave-drill operated in similar conditions.

The relatively low power needed for open-end coaxial applicators to reach LMH intensification in millimeter scales (typically below ~0.2 kW) makes solid-state generators (*e.g.* LDMOS [42]) suitable as sources for LMH applicators. These compact schemes enable a new range of portable LMH intensifiers.

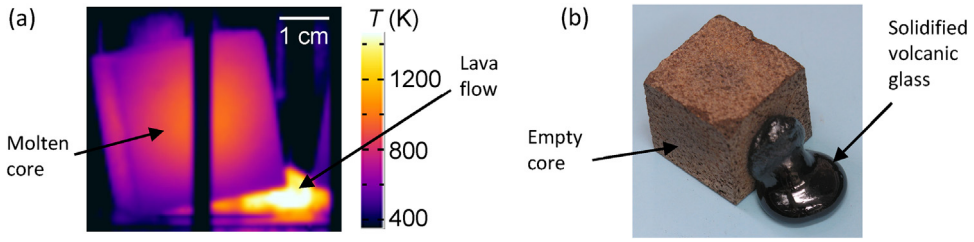

Fig. 6. A basalt brick irradiated in a microwave cavity [52]: (a) The intensified LMH melts only the core as observed through the porous surfce, which remains solid. The lava flow ejected from the core tilts the brick in the cavity. (b) The hollow brick with the lava solidified to volcanic glass (obsidian).

3.3. Plasma ejection from solids

Dusty plasmas in forms of fireballs and fire-columns can be ejected by LMH directly from hotspots evolved in solid substrates, as presented *e.g.* in Refs. [35–39] for various dielectric and metallic materials. The intensified LMH-plasma process begins with a hotspot formation as presented above (*e.g.* for microwave drilling). However, for plasma ejection the electrode is lifted up (rather than pushed in) in order to detach the molten drop from the surface, and to further inflate it to a form of a buoyant fireball.

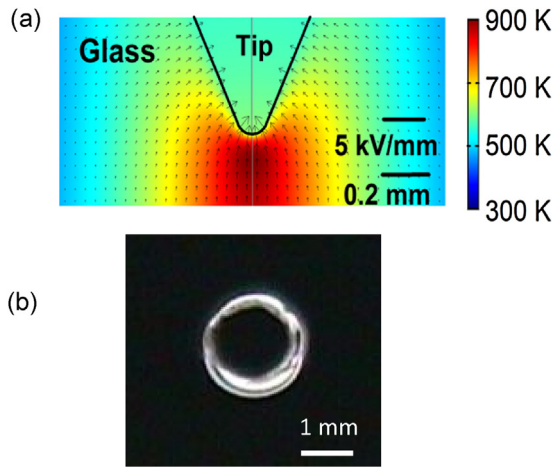

Fig. 7. LMH intensification in glass irradiated by a coaxial open-end applicator using an LDMOS-based microwave-drill [42]: (a) The simulated spatial temperature and electric-field distributions at the hotspot, and (b) an image of a ~1.2-mm$^{\varnothing}$ hole made by LMH in glass.

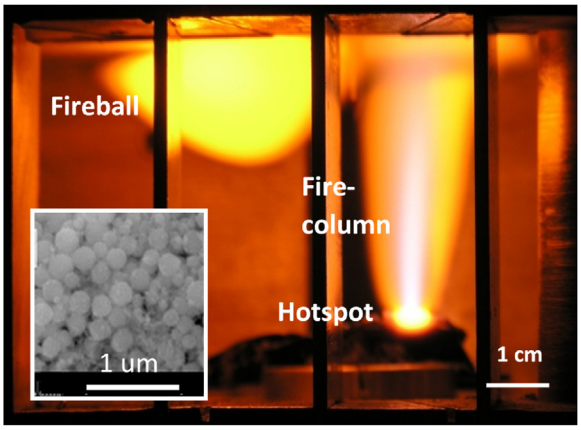

Fig. 8. Plasmoids ejected from an LMH hotspot in glass. This image captures together the intensified hotspot in the solid substarte, the fire-column ejected, and the secondary fireball evolved (each may solely exists in other operating modes). The inset shows nano-particles produced by LMH generated dusty plasma, as observed by SEM [38].

Beside their resemblance to natural ball-lightning phenomena, fireballs and fire-columns, as shown in Fig. 8, may also have practical importance, *e.g.* as means to produce nano-particles directly from various substrate materials, such as silicon, glass, ceramics, copper, titanium, *etc.* [36–39]. Nanoparticles were observed in these and other materials, both by *in-situ* synchrotron small-angle X-ray scattering (SAXS) of the dusty plasma, and by *ex-situ* SEM observations of the nano-powders collected after the processes. Particles of various sizes, shapes, and number densities have been obtained, as described in Refs. [36–39] (typically of $<0.1\,\mu m$ size and $\sim 10^{16}\,m^{-3}$ number density within the dusty plasma). The LMH generated plasma can also be used for material identification [46] by atomic emission spectroscopy of the light emitted by the plasma ejected from the hotspot (similarly to the laser induced breakdown spectroscopy (LIBS)).

3.4. LMH of metal powders

Coupling mechanisms of microwaves and metal powders are known in the literature in various volumetric schemes [54,55]. Recent experiments show that metal powders with negligible dielectric losses can also be effectively heated and incrementally solidified by localized microwaves [44]. This LMH effect is attributed to the time-varying magnetic component of the EM field, and to the eddy currents induced in the metal-powder particles, as illustrated in Fig. 9a [55]. This effect is intensified by the micro-powder geometry, and it also occurs in diamagnetic metals such as copper. The heat is generated due to the metal electric resistivity, which impedes the eddy currents.

In magnetic-like heating of metallic powders, the LMH effect is not characterized by thermal-runaway instability since the temperature tends to stabilize at ~700 K due to the particles' necking and consolidation effects [54]. Experimental and simulation results of LMH experiments in bronze-based powder are presented in [44].

3.5. LMH ignition of thermite in air and underwater

Powder mixtures, such as of pure aluminum and magnetite (or hematite) powders, may generate energetic thermite reactions. These could be useful for a variety of combustion and material processing applications. However, their usage is yet limited by the difficult ignition of these reactions. It was recently found that ignition of thermite reactions is feasible by intensified LMH [43]. The power required for thermite ignition by LMH is ~0.1-kW for a ~3-s period, which could be provided by a solid-state microwave generator.

The thermite mixture exhibits both dielectric and magnetic loss mechanisms. The magnetic LMH is implemented by a short-end applicator, which enhances the magnetic field in front of it. It yields a faster heating rate than the open-end, dielectric-LMH applicator,

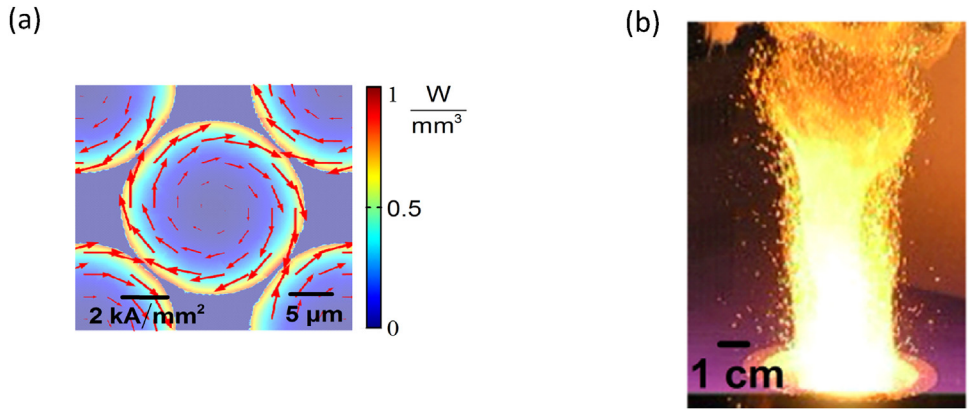

Fig. 9. LMH of metallic powders: (a) Eddy currents induced in copper powder [55]. (b) A thermite flame ignited by LMH intensification [43].

up to the Curie temperature at 858 K, where the magnetic losses significantly decrease. Integrating both magnetic and electric LMH mechanisms by a hybrid applicator enables the thermal-runaway instability and the thermite ignition [43]. These experiments also demonstrate the feasibility of cutting and welding by relatively low-power LMH. The initiation of the intense exothermic reaction in thermites, as shown in Fig. 9b, also demonstrates an example for LMH ignition of other high-temperature self-propagating syntheses (SHS) [56].

Due to their zero-oxygen balance, exothermic thermite reactions may also occur underwater. However, this feature is also difficult to utilize because of the hydrophobic properties of the thermite powder, and its tendency to agglomerate on the water surface, rather than to sink into the water. The recently discovered bubble-marble (BM) effect [57] enables the insertion and confinement of a thermite-powder batch into water by a static magnetic field, and its ignition by LMH underwater [58]. Potential applications of this underwater combustion effect may include wet welding, thermal drilling, detonation, thrust generation, material processing, and composite-material production. These could be implemented in other oxygen-free environments as well, such as the outer space.

3.6. Surface treatment and doping

Chemical reactions applied by LMH intensification for surface treatments also include thermite reactions for the conversion of rust to iron and alumina [43]. Another example is the local doping of silicon substrates by LMH, studied using silver and aluminum dopants [34]. The dopant material is incorporated in these processes in the electrode tip, and is diffused into the locally heated bulk to form a sub-micron PN junction. These shallow LMH techniques open new possibilities for a variety of surficial treatments and local surface processing.

3.7. LMH potential for 3D printing

The LMH effect in metal powders is also associated with internal micro-plasma breakdowns between the particles, which leads to local melting and solidification of the metal powder. This effect enables a potential technique for stepwise 3D printing and additive manufacturing (AM) [44]. The consolidated drop of metal powder is placed in this technique as a building block on top of the previously constructed structure in a stepwise AM process, as illustrated in Fig. 10a. A rod constructed by LMH-AM from bronze-based powder in 14 steps is shown in Fig. 10b [44]. A similar process using magnetic fixation of iron powder is also presented in [44].

4. Discussion

The various LMH aspects reviewed in this paper differ from the common microwave-heating paradigm by the intentional concentration and local intensification of the microwave-heating energy into a HAZ much smaller in size than the microwave wavelength. The relatively high power density concentrated within this small volume enables the hotspot melting, evaporation, and even breakdown to plasma.

LMH intensification is applicable to dielectrics and metals as well, in solid, powder, and liquid forms. LMH does not require a cavity or an enclosed chamber, and it can be implemented by conventional low-cost microwave generators. In the low-power regime, LMH can also be implemented by solid-state generators [42].

The LMH intensification technique can be considered, to some limited extent, as a low-end substitute for laser-based applications, such as drilling and cutting [11–17], joining [59], surface treatment [34,43], material identification [39], and additive manufacturing [44]. While LMH may provide low-cost, compact and efficient

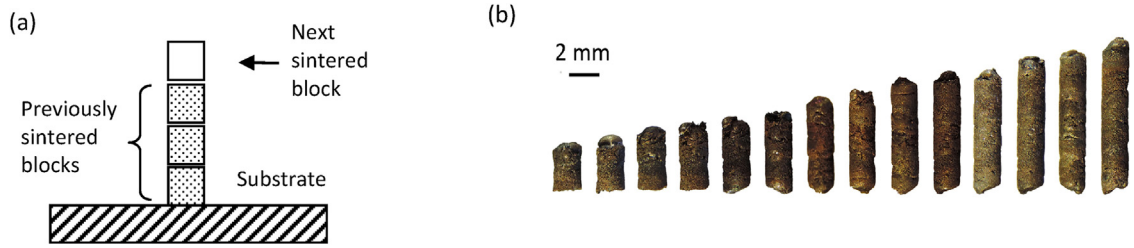

Fig. 10. Additive manufacturing (3D printing) of metal powders by LMH [44]: (a) A conceptual scheme of the stepwise LMH-AM process. (b) A 2-mm$^{\Phi}$ rod constructed in 14 consequent steps from bronze-based powder.

solutions in this regard, it still requires a physical contact with the object. Its resolution (~1 mm) is yet inferior with respect to lasers. Therefore, one may expect that LMH intensification will find applications in operating regimes of relatively large volumes and rough processes, as a complementary means to the relatively more accurate and expensive laser-based systems.

The LMH approach conceptually differs from the well-established volumetric microwave-heating technologies. The LMH intensification requires different mechanisms, theoretical considerations, and technical implementations, and it addresses other needs than the uniform microwave heating. As such, the various LMH phenomena, models and techniques, reviewed herein a unified holistic approach, form together a new paradigm [47–49] which expands the field of microwave heating to relatively small but much more intensified HAZ's.

Acknowledgements

The author thanks Dr. Yehuda Meir for fruitful discussions. This research was supported in part by the Israel Science Foundation (Grant Nos. 1270/04, 1639/11, and 1896/16).

References

[1] A.C. Metaxas, Foundations of Electroheat: A Unified Approach, John Wiley & Sons Ltd., Chichester, 1996.
[2] S. Chandrasekaran, S. Ramanathan, T. Basak, Microwave material processing—a review, AIChE J. 58 (2012) 330–363.
[3] R. Vadivambal, D.S. Jayas, Non-uniform temperature distribution during microwave heating of food materials – a review, Food Bioprocess Technol. 3 (2010) 161–171.
[4] K. Pitchai, S.L. Birla, D. Jones, J. Subbiah, Assessment of heating rate and non-uniform heating in domestic microwave ovens, J. Microwave Power Electromagn. Energy 46 (2012) 229–240.
[5] Z.Y. Li, R.F. Wang, T. Kudra, Uniformity issue in microwave drying, Dry. Technol. 29 (2011) 652–660.
[6] G. Roussy, A. Bennani, J. Thiebaut, Temperature runaway of microwave irradiated materials, J. Appl. Phys. 62 (1987) 1167–1170.
[7] G.A. Kriegsmann, Thermal runaway in microwave heated ceramics: a one-dimensional model, J. Appl. Phys. 71 (1992) 1960–1966.
[8] C.A. Vriezinga, S. Sánchez-Pedreño1, J. Grasman, Thermal runaway in microwave heating: a mathematical analysis, Appl. Math. Model. 26 (2002) 1029–1038.
[9] V. Yakovlev, S.M. Allan, M.L. Fall, H.S. Shulman, Computational study of thermal runaway in microwave processing of zirconia, Proc. Ampere 13th Conf., pp. 303–306, Sept. 5–8, 2011, Toulouse, France, 2017.
[10] Y. Alpert, E. Jerby, Coupled thermal-electromagnetic model for microwave heating of temperature-dependent dielectric media, IEEE Trans. Plasma Sci. 27 (1999) 555–562.
[11] E. Jerby, V. Dikhtyar, O. Actushev, U. Grosglick, The microwave drill, Science 298 (2002) 587–589.
[12] E. Jerby, O. Aktushev, V. Dikhtyar, Theoretical analysis of the microwave-drill near-field localized heating effect, J. Appl. Phys. 97 (2005) 1–7 (Art. No. 034909).
[13] E. Jerby, V. Dikhtyar, Drilling into hard non-conductive materials by localized microwave radiation, 8th int'l conf. microwave & high-frequency heating, bayreuth, sept. 4–7, in: M. Willert-Porada (Ed.), Advances in Microwave and Radio-Frequency Processing, Springer, 2006, pp. 687–694.
[14] E. Jerby, O. Aktushev, V. Dikhtyar, P. Livshits, A. Anaton, T. Yacoby, A. Flax, A. Inberg, D. Armoni, Microwave drill applications for concrete, glass and silicon, Proc. 4th World Congress Microwave & Radio-Frequency Applications, Pp. 156–165, Nov. 7–12, Austin, Texas, 2004.
[15] E. Jerby, V. Dikhtyar, O. Aktushev, Microwave drill for ceramics, Am. Ceram. Soc. Bull. 82 (2003) 35–37.
[16] X. Wang, W. Liu, H. Zhang, S. Liu, Z. Gan, Application of microwave drilling to electronic ceramics machining, 7th Int'l Conf. Electronics Packaging Technology, Proc. Article # 4198945, pp. 1–4, Aug. 26–29, Shanghai, China, 2006.
[17] E. Jerby, A.M. Thompson, Microwave drilling of ceramic thermal barrier coatings, J. Am. Ceram. Soc. 87 (2004) 308–310.
[18] J.B.A. Mitchell, E. Jerby, Y. Shamir, Y. Meir, J.L. LeGarrec, M. Sztucki, Rapid internal bubble formation in a microwave heated polymer observed in real-time by X-ray scattering, Polym. Degrad. Stabil. 96 (2011) 1788–1792.
[19] R. Herskowits, P. Livshits, S. Stepanov, O. Aktushev, S. Ruschin, E. Jerby, Silicon heating by a microwave-drill applicator with optical interferometric thermometry, Semicond. Sci. Technol. 22 (2007) 863–869.
[20] G. Wang, P. Radziszewski, J. Ouellet, Particle modeling simulation of thermal effects on ore breakage, Comput. Mater. Sci. 43 (2008) 892–901.
[21] N.R. Lippiatt, F.S. Bourgeois, Recycling-oriented investigation of local porosity changes in microwave heated-concrete, KONA Powder Particle J. 31 (2014) 247–264.
[22] A. Copty, F. Sakran, M. Golosovsky, D. Davidov, A. Frenkel, Low power near-field microwave applicator for localized heating of soft matter, Appl. Phys. Lett. 84 (2004) 5109–5111.
[23] Y. Eshet, R. Mann, A. Anaton, T. Yacoby, A. Gefen, E. Jerby, Microwave drilling of bones, IEEE Trans. Biomed. Eng. 53 (2006) 1174–1182.
[24] T.Z. Wong, B.S. Trembly, A theoretical model for input impedance of interstitial microwave antennas with choke, Int. J. Radiat. Oncol. Biol. Phys. 28 (1994) 673–682.
[25] I. Longo, G.B. Gentili, M. Cerretelli, N. Tosoratti, A coaxial antenna with miniaturized choke for minimally invasive interstitial heating, IEEE Trans. Biomed. Eng. 50 (2003) 82–88.
[26] C.L. Brace, Microwave ablation technology: what every user should know, Curr. Prob. Diagn. Radiol. 38 (2009) 61–67.
[27] J. Yoon, J. Cho, N. Kim, D.-D. Kim, E. Lee, C. Cheon, Y. Kwon, High-frequency microwave ablation method for enhanced cancer treatment with minimized collateral damage, Int. J. Cancer 129 (2011) 1970–1978.
[28] P. Keangin, P. Rattanadecho, Analysis of heat transport on local thermal non-equilibrium in porous liver during microwave ablation, Int. J. Heat Mass Trans. 67 (2013) 46–60.
[29] A. Kempitiya, D.A. Borca-Tasciuc, H.S. Mohamed, M.M. Hella, Localized microwave heating in micro-wells for parallel DNA amplification applications, Appl. Phys. Lett. 94 (2009) 1–3 (Art. No. 064106).
[30] F. Marken, Chemical and electro-chemical applications of in situ microwave heating, Annu. Rep. Prog. Chem. Sect. C 104 (2008) 124–141.
[31] Y. Tsukahara, A. Higashi, T. Yamauchi, T. Nakamura, M. Yasuda, A. Baba, Y. Wada, In situ observation of nonequilibrium local heating as an origin of special effect of microwave on chemistry, J. Phys. Chem. C 114 (2010) 8965–8970.
[32] G.B. Gentili, M. Linari, I. Longo, A.S. Ricci, A coaxial microwave applicator for direct heating of liquids filling chemical reactors, IEEE Trans. Microwave Theory Tech. 57 (2009) 2268–2275.
[33] I. Longo, A.S. Ricci, Chemical activation using an open-end coaxial applicator, J. Microwave Power Electromagn. Energy 41 (2007) 4–19.
[34] P. Livshits, V. Dikhtyar, A. Inberg, A. Shahadi, E. Jerby, Silicon doping by a point-contact microwave applicator, Microelectron. Eng. 88 (2011) 2831–2836.
[35] V. Dikhtyar, E. Jerby, Fireball ejection from a molten hot-spot to air by localized microwaves, Phys. Rev. Lett. 96 (2006) 1–4 (Art. No. 045002).
[36] J.B. Mitchell, J.L. LeGarrec, M. Sztucki, T. Narayanan, V. Dikhtyar, E. Jerby, Evidence for nanoparticles in microwave-generated fireballs observed by synchrotron X-ray scattering, Phys. Rev. Lett. 100 (2008) 1–4 (Art. No. 065001).
[37] E. Jerby, A. Golts, Y. Shamir, S. Wonde, J.B.A. Mitchell, J.L. LeGarrec, T. Narayanan, M. Sztucki, D. Ashkenazi, Z. Barkay, Nanoparticle plasma ejected directly from solid copper by localized microwaves, Appl. Phys. Lett. 95 (2009) 191501 (Art. No. 191501).
[38] Y. Meir, E. Jerby, Z. Barkay, D. Ashkenazi, J.B.A. Mitchell, T. Narayanan, N. Eliaz, J.-L. LeGarrec, M. Sztucki, O. Meshcheryakov, Observations of ball-lightning-like plasmoids ejected from silicon by localized microwaves, Materials 6 (2013) 4011–4030.
[39] S. Popescu, E. Jerby, Y. Meir, Z. Barkay, D. Ashkenazi, J.B.A. Mitchell, J.-L. Le Garrec, T. Narayanan, Plasma column and nano-powder generation from solid titanium by localized microwaves in air, J. Appl. Phys. 118 (2015) (Art. No 023302).
[40] N. Sabelstrom, M. Hayashi, T. Watanabe, K. Nagata, Observation of localized heating phenomena during microwave heating of mixed powders using in situ x-ray diffraction technique, J. Appl. Phys. 116 (2014) 164902.
[41] A. Toossi, H. Moghadas, M. Shayegh, D. Sameoto, M. Daneshmand, Efficient microwave susceptor design for localized heating on substrate, IEEE Trans. Compon. Packag. Manuf. Technol. 5 (2015) 570–578.
[42] Y. Meir, E. Jerby, Localized rapid heating by low-power solid-state microwave-drill, IEEE Trans. Microwave Theory Tech. 60 (2012) 2665–2672.
[43] Y. Meir, E. Jerby, Thermite-powder ignition by electrically-coupled localized microwaves, Combust. Flame 159 (2012) 2474–2479.
[44] E. Jerby, Y. Meir, A. Salzberg, E. Aharoni, A. Levy, J. Planta Torralba, B. Cavallini, Incremental metal-powder solidification by localized microwave-heating and its potential for additive manufacturing, Addit. Manuf. 6 (2015) 53–66.
[45] O. Wiedenmann, R. Ramakrishnan, P. Saal, E. Kılıç, U. Siart, T.F. Eibert, W. Volk, Local microwave heating of sand molds as a means to overcome design limitations in sand mold casting, Adv. Radio Sci. 12 (2014) 21–28.
[46] Y. Meir, E. Jerby, Breakdown spectroscopy induced by localized microwaves for material identification, Microwave Opt. Technol. Lett. 53 (2011) 2281–2283.
[47] E. Jerby, Localized microwave-heating (LMH) model and potential applications, Proc. 3rd Global Congress on Microwave-Energy Applications, 3GCMEA, Cartagena, Spain, July 25–29, 2016.
[48] Y. Meir, E. Jerby, The localized microwave-heating (LMH) paradigm – theory, experiments, and applications, Proc. 2nd Global Congress on Microwave-Energy Applications, 2GCMEA, pp. 131–145, Long Beach, California, July 23–27, 2012.
[49] Y. Meir, E. Jerby, The localzied microwave-heating (LMH) paradigm – thoery, observations, and applications, Proc. 15th Int'l Conf. Microwave & High-Frequency Heating, AMPERE 2015, Krakow, Poland, Sept. 14–17, 2015.
[50] E. Jerby, A. Gover, Wave profile modification in Raman free-electron lasers: space-charge transverse fields and optical guiding, Phys. Rev. Lett. 63 (1989) 864–867.

[51] Z. Menachem, E. Jerby, Transfer matrix function (TMF) for wave propagation in dielectric waveguides with arbitrary transverse profiles, IEEE Trans. Microwave Theory Tech. 46 (1998) 975–982.
[52] E. Jerby, Y. Meir, M. Faran, Basalt melting by localized-microwave thermal-runaway instability, Proc. AMPERE 14th Int'l Conf. Microwave & High Frequency Heating, pp. 255–258, Nottingham, UK, Sept. 16–19, 2013.
[53] E. Jerby, Y. Shamir, R. Peleg, Y. Aharoni, A silent mechanically-assisted microwave-drill for concrete with integrated adaptive impedance matching, Proc. AMPERE 14th Int'l Conf. Microwave & High-Frequency Heating, pp. 267–270, Nottingham, UK, Sept. 16–19, 2013.
[54] D.C. Dube, P.D. Ramesh, J. Cheng, M.T. Lanagan, D. Agrawal, R. Roy, Experimental evidence of redistribution of fields during processing in a high-power microwave cavity, Appl. Phys. Lett. 85 (2004) (3632-3624).
[55] T. Galek, K. Porath, E. Burkel, U. Van Rienen, Extraction of effective permittivity and permeability of metallic powders in the microwave range, Modell. Simul. Mater. Sci. Eng. 18 (2010) 1–13 (Art. No. 025015).
[56] R. Rosa, P. Veronesi, C. Leonelli, A review on combustion synthesis intensification by means of microwave energy,", Chem. Eng. Process. 71 (2013) 2–18.
[57] Y. Meir, E. Jerby, Insertion and confinement of hydrophobic metallic powder in water: the bubble-marble effect, Phys. Rev. E 90 (2014) 1–4 Art. No. 030301 (R).
[58] Y. Meir, E. Jerby, Underwater microwave ignition of hydrophobic thermite powder enabled by the bubble-marble effect, Appl. Phys. Lett. 107 (2015) 1–4 (Art. No. 054101).
[59] N. Kondo, H. Hyuga, H. Kita, K. Hirao, Joining of silicon nitride by microwave local heating, J. Ceram. Soc. Jpn. 118 (2010) 959–962.